Energetic electron precipitation from the outer radiation belt during geomagnetic storms

Richard B. Horne,[1,2] Mai Mai Lam,[1] and Janet C. Green[3]

Received 28 July 2009; revised 1 September 2009; accepted 10 September 2009; published 9 October 2009.

[1] Relativistic electron precipitation changes the chemistry of the upper atmosphere and depletes ozone, but the spatial and temporal distributions are poorly known. Here we survey more than 9 years of data from low altitude satellites for different phases of geomagnetic storms. We find that for the outer radiation belt, electron precipitation >300 keV peaks during the main phase of storms whereas that >1 MeV peaks during the recovery phase. Precipitation >300 keV can occur at all geographic longitudes in both hemispheres whereas that >1 MeV occurs mainly poleward of the South Atlantic anomaly (SAA) region. The data suggest that wave-particle interactions are strong enough to precipitate >300 keV electrons into the bounce loss cone, but precipitate >1 MeV electrons into the drift loss cone. We find that whistler mode chorus waves alone cannot account for the higher MeV precipitation flux during the recovery phase. We suggest that whistler mode chorus waves accelerate electrons up to MeV energies during the recovery phase which are then precipitated by EMIC waves. The effects on atmospheric chemistry due to MeV electron precipitation are more likely to occur in the southern hemisphere poleward of the SAA region with a delay of 1–2 days or more from the peak of the storm.
Citation: Horne, R. B., M. M. Lam, and J. C. Green (2009), Energetic electron precipitation from the outer radiation belt during geomagnetic storms, *Geophys. Res. Lett.*, *36*, L19104, doi:10.1029/2009GL040236.

1. Introduction

[2] During geomagnetic storms the flux of relativistic electrons >1 MeV in the Van Allen radiation belts can vary by up to five orders of magnitude. These variations are hazardous to satellites as they can result in malfunctions, and in extreme cases total loss resulting in insurance claims of hundreds of millions of dollars [*Baker et al.*, 1998]. Precipitation from the radiation belts also depletes ozone [*Thorne*, 1977] which may affect climate [e.g., *Rozanov et al.*, 2005].

[3] During the main phase of geomagnetic storms rapid reductions or 'drop-outs' in the relativistic electron flux may occur for 10 hours or more [*Onsager et al.*, 2002]. These drop-outs may be partly due to adiabatic transport effects [*Kim and Chan*, 1997] but since this process is reversible it does not explain storm time variations [*Reeves et al.*, 2003]. Alternatively, losses could be due to rapid outward electron transport [*Shprits et al.*, 2006] or enhanced precipitation into the atmosphere due to wave-particle interactions [e.g., *Millan and Thorne*, 2007]. Recent calculations suggest that the radiation belt could be depleted on timescales of 1 hour or so [*Selesnick*, 2006], although data suggests a much longer timescale for electron loss >800 keV (C. J. Rodger et al., Use of POES SEM-2 observations to examine radiation belt dynamics and energetic electron precipitation into the atmosphere, submitted to *Journal of Geophysical Research*, 2009). While it is almost impossible to measure the precipitating flux near the magnetic equator due to the smallness of the loss cone, recently it has been shown that the low altitude Polar Orbiting Environmental Satellites (POES) can measure the trapped and precipitating electron flux at energies >1 MeV [*Sandanger et al.*, 2009]. Here we utilize this new development to determine the global extent of electron precipitation >300 keV and >1 MeV during the different phases of geomagnetic storms.

2. Storm Time Variations

[4] We used the Dst index to define geomagnetic storms since it has a well defined signature [*Gonzalez et al.*, 1994]. Dst is a measure of the electrical current systems, such as the ring current and magnetopause currents, that develop during a magnetic storm. We used a 12 hour running mean of the hourly Dst index to smooth the data and identified storms for Dst ≤ -70 nT, which corresponds to moderate to strong storms or larger [*Loewe and Prölss*, 1997]. From the minimum Dst we tracked back in time to find when Dst dropped below -35 nT and forwards in time to find when Dst rose above -35 nT. These values were used to define the main and recovery phase, respectively. The pre-storm period was defined as 24 hours before Dst first dropped below -35 nT, and provided there was no storm in the previous 48 hours. The procedure was carried out for the period 1998 to 2007, corresponding to when the NOAA 15, 16, 17 and 18 satellites were operating with a new generation of particle detector. 69 storms were identified.

[5] This method omits a very important class of weak long duration storms associated with co-rotating interaction (CIR) regions in the solar wind [*Tsurutani et al.*, 2006]. They usually have a minimum Dst > -75 nT and will be treated separately elsewhere.

[6] Data from the medium energy proton and electron detector (MEPED) on NOAA 15, 16, 17 and 18 were used in our analysis. The satellites are in a low altitude (815 km) sun synchronous polar orbit with a period of approximately 100 minutes. MEPED includes two solid state detectors, one pointing radially outwards along the Earth satellite

[1]British Antarctic Survey, Cambridge, UK.
[2]Also at Department of Automatic Control and Systems Engineering, University of Sheffield, Sheffield, UK.
[3]Space Weather Prediction Center, National Oceanic and Atmospheric Administration, Boulder, Colorado, USA.

0094-8276/09/2009GL040236$05.00

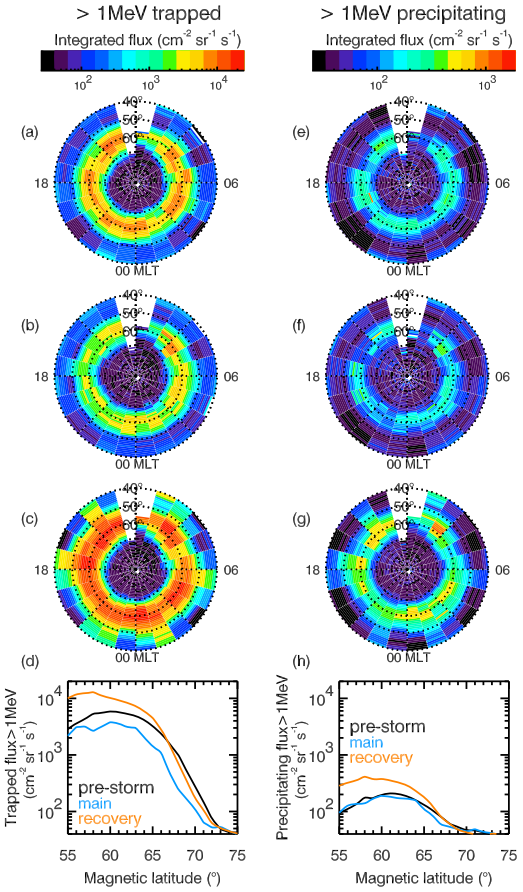

Figure 1. (left) Trapped and (right) precipitating electron flux >1 MeV in the Southern hemisphere as a function of MLT and magnetic latitude for (a and e) pre-storm, (b and f) main, and (c and g) recovery storm phase and (d and h) averaged over MLT.

direction, (0° detector), and the other at 90° to this direction, antiparallel to the spacecraft velocity. Since the opening angle is ±15°, the 0° detector measures the precipitating flux inside the bounce loss cone for approximately $L \geq 1.4$ (Rodger et al., submitted manuscript, 2009) while the 90° detector measures the trapped electron flux. Data from the >6.9 MeV proton channel was used to measure >1 MeV electrons [see *Sandanger et al.*, 2009] together with the >30, >100 and >300 keV electron channels. Data collected during solar proton events were omitted and corrections to remove other proton contamination were applied (for more details see M. M. Lam et al. (Origin of energetic electron precipitation >30 keV into the atmosphere, submitted to *Journal of Geophysical Research*, 2009)). The data were collected into bins of 1 hour in magnetic local time (MLT) and 1° magnetic latitude according to the phase of each magnetic storm.

[7] Figure 1 shows the >1 MeV electron flux in the southern hemisphere for different phases of magnetic storms. The trapped flux (left column) decreases during the main phase at all local times and then increases in the recovery phase above the pre-storm level. The flux does not show any significant variation with MLT which suggests that there is no localized rapid loss (or acceleration) process operating on timescales less than the drift time. Although there is a decrease in flux during the main phase, by about a factor of 2, the drop-out is not a strong feature (bottom left). Large flux drop outs often occur during CIR driven storms [*Borovsky and Denton*, 2009] and other individual CME driven storms [e.g., *Brautigam and Albert*, 2000] but is not so apparent here due to the averaging process. On average there is a net increase in >1 MeV trapped electron flux associated with magnetic storms.

[8] In contrast to the trapped flux the precipitating flux (right column) remains almost the same during the pre-storm and main phase. The data show little or no evidence that the reduction in the trapped flux during the main phase is due to precipitation into the atmosphere. Instead precipitation increases during the recovery phase, which is surprising since this is when the trapped flux is generally increasing. The precipitating flux is more than an order of magnitude less than the trapped flux which suggests weak diffusion into the loss cone on average, although strong diffusion may occur locally for limited MLT.

[9] This behavior in the MeV electron flux is different to that at lower energies. Figure 2 shows that there is very little variation in the trapped flux >300 keV between the pre-storm and main phase. The trapped flux increases during the recovery phase, mainly at lower magnetic latitudes (bottom left panel), and there is no marked asymmetry in MLT. This is consistent with inward radial diffusion and gradient and curvature drift around the Earth at these energies. However, the precipitating flux >300 keV increases significantly

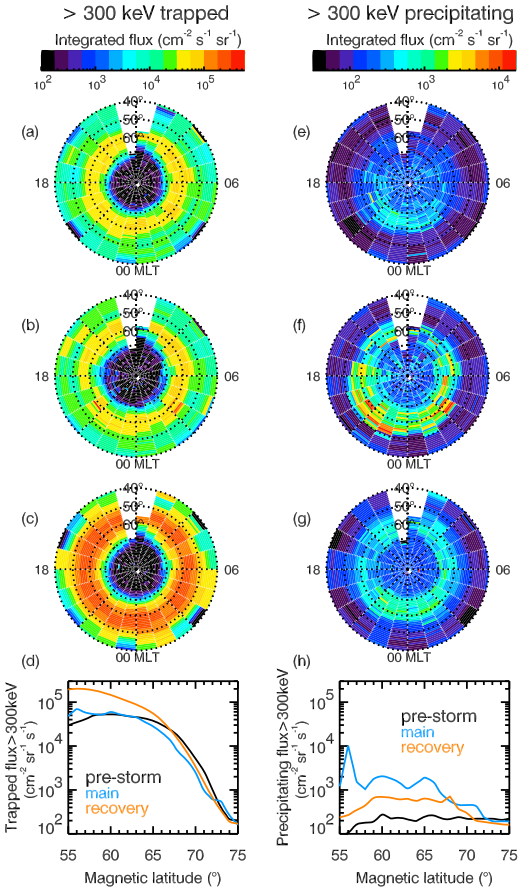

Figure 2. Same as Figure 1 but for >300 keV.

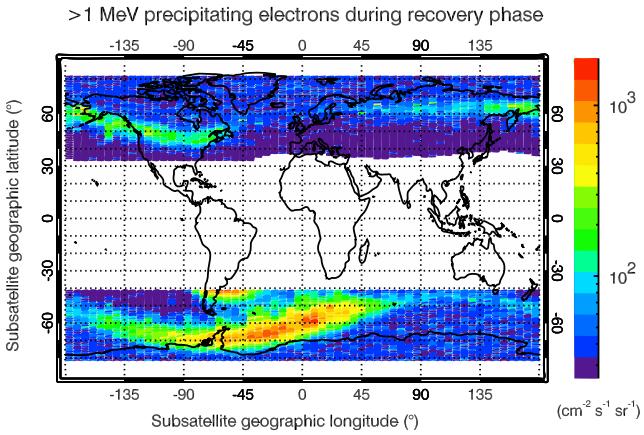

Figure 3. Electron precipitation >1 MeV. The small red region over South America is contaminated by protons and is not considered.

during the main phase and although it becomes lower during the recovery phase it still remains much higher than the pre-storm level. The ratio of the precipitating to trapped flux is highest during the main phase and depends on latitude.

3. South Atlantic Anomaly

[10] The data raise questions as to why electron precipitation >300 keV peaks during storm main phase while that >1 MeV peaks during the recovery phase, and whether there is an important different in the wave-particle interactions responsible?

[11] In the southern hemisphere there is a weakness in the Earth's magnetic field known as the south Atlantic Anomaly (SAA). Data at low L, corresponding to the inner radiation belt, is contaminated by protons in the SAA region but the weakness extends poleward over the outer radiation belt where contamination is not an issue. Figure 3 shows that precipitation >1 MeV during the recovery phase is significantly higher over the Antarctic peninsular region, poleward of the SAA and corresponding to the outer radiation belt. There is very little precipitation at other longitudes, or into the northern hemisphere (similarly for the main phase, not shown). Conversely, during the main phase electron precipitation >300 keV is not restricted poleward of the SAA region, but can occur at all geographic longitudes (Figure 4, and similarly for the recovery phase, not shown). Furthermore, precipitation into the northern hemisphere is almost as strong as that into the southern hemisphere.

4. Discussion and Conclusions

[12] The fact that >300 keV precipitation can occur at all geographic longitudes suggests that pitch angle scattering is strong enough to scatter electrons into the bounce loss cone and cause precipitation at any longitude. One consequence of this is that the distribution of >300 keV precipitation in Figure 2 is more likely to show where pitch angle scattering of >300 keV electrons takes place in MLT. Waves responsible for pitch angle scattering MeV electrons, even if they are restricted in MLT, may also facilitate precipitation of 300 keV electrons [*Shprits et al.*, 2009]. However, the fact that precipitation >1 MeV is restricted in geographic longitude suggests that >1 MeV electrons are mainly scattered into the drift loss cone and drift around the Earth to the SAA where they are lost to the atmosphere. Thus we suggest that the MLT distribution of >1 MeV precipitation (Figure 1g) indicates where the SAA is in relation to MLT rather than the presence of strong wave-particle interactions at that location.

[13] The question arises as to whether the waves responsible for precipitating >300 keV electrons also precipitate >1 MeV electrons? We argue that this is unlikely. Whistler mode chorus waves are one of the strongest candidates for precipitating 10 keV to a few MeV electrons since they can resonate with electrons over this energy range [*Horne et al.*, 2005]. Pitch angle diffusion into the loss cone becomes less effective at higher energies. Consequently diffusion into the loss cone is very small at ~1 MeV and the waves are more effective at accelerating trapped electrons at high energies [*Horne et al.*, 2005; *Shprits et al.*, 2006; *Varotsou et al.*, 2005]. Even so, if chorus wave power increases one would expect precipitation >300 keV and >1 MeV to increase, but this is not observed.

[14] The other possibility is that there is some additional scattering at higher energies during the recovery phase that does not scatter 300 keV electrons very effectively. Fast magnetosonic waves can contribute to pitch angle scattering at MeV energies but cannot diffuse electrons into the loss cone on their own [*Horne et al.*, 2007]. Electromagnetic ion cyclotron (EMIC) waves can scatter electrons with energies >500 keV [*Summers and Thorne*, 2003; *Albert*, 2003]. They are observed near dusk and on the dayside [*Meredith et al.*, 2003]. However, unless the plasma density is very high, such as inside the plasmapause or in high density plumes on the dayside, EMIC waves generally scatter electrons greater than a few MeV or more. The waves are excited by a temperature anisotropy in the proton distribution that is injected during the main phase and forms the ring current. If these waves are responsible for the additional scattering at a few MeV, the question is why is the precipitation not observed during the main phase. Ground based observations in the Antarctic show that EMIC waves are mainly observed during the recovery phase [*Engebretson et al.*, 2008], but

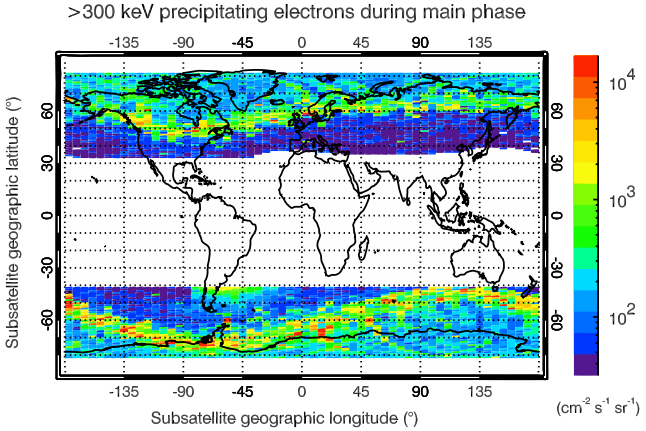

Figure 4. Same as Figure 3 but for >300 keV.

these observations do not rule out their presence during the main phase since the ionosphere may be so disturbed that the waves cannot reach the ground.

[15] We suggest that the reason why >1 MeV precipitation is higher during the recovery phase is a consequence of how the radiation belt is reformed during storms. The new concept recently put forward [*Horne*, 2007] is that convection, substorms, and inward radial diffusion transport electrons inward at energies up to a few hundred keV. These form unstable distributions that excite whistler mode chorus waves which further accelerate electrons up to several MeV. However, it takes 1–2 days to accelerate the electrons up to a few MeV. Thus EMIC waves would be more effective in precipitating >1 MeV electrons during the recovery phase after the electrons had had time to be accelerated. In effect the chorus waves accelerate the electrons up to energies of a few MeV whereupon EMIC waves precipitate them.

[16] The data show that the largest change in chemistry due to MeV electron precipitation should occur in the southern hemisphere poleward of the SAA region and should occur during the recovery phase of storms. Thus chemistry climate models should take into account a 1–2 day delay in MeV electron precipitation and higher MeV fluxes poleward of the South Atlantic when modelling the atmospheric response to geomagnetic storms and solar variability.

[17] **Acknowledgment.** This research was supported in the UK by the Natural Environment Research Council.

References

Albert, J. M. (2003), Evaluation of quasi-linear diffusion coefficients for EMIC waves in a multispecies plasma, *J. Geophys. Res.*, *108*(A6), 1249, doi:10.1029/2002JA009792.

Baker, D. N., J. H. Allen, S. G. Kanekal, and G. D. Reeves (1998), Disturbed space environment may have been related to pager satellite failure, *Eos Trans. AGU*, *79*, 477.

Borovsky, J. E., and M. H. Denton (2009), Relativistic-electron dropouts and recovery: A superposed epoch study of the magnetosphere and the solar wind, *J. Geophys. Res.*, *114*, A02201, doi:10.1029/2008JA013128.

Brautigam, D. H., and J. M. Albert (2000), Radial diffusion analysis of outer radiation belt electrons during the October 9, 1990, magnetic storm, *J. Geophys. Res.*, *105*, 291–309.

Engebretson, M. J., et al. (2008), Pc1-Pc2 waves and energetic particle precipitation during and after magnetic storms: Superposed epoch analysis and case studies, *J. Geophys. Res.*, *113*, A01211, doi:10.1029/2007JA012362.

Gonzalez, W. D., J. A. Joselyn, Y. Kamide, H. W. Kroehl, G. Rostoker, B. T. Tsurutani, and V. M. Vasyliunas (1994), What is a geomagnetic storm?, *J. Geophys. Res.*, *99*, 5771–5792.

Horne, R. B. (2007), Plasma astrophysics: Acceleration of killer electrons, *Nat. Phys.*, *3*, 590–591.

Horne, R. B., R. M. Thorne, S. A. Glauert, J. M. Albert, N. P. Meredith, and R. R. Anderson (2005), Timescale for radiation belt electron acceleration by whistler mode chorus waves, *J. Geophys. Res.*, *110*, A03225, doi:10.1029/2004JA010811.

Horne, R. B., R. M. Thorne, S. A. Glauert, N. P. Meredith, D. Pokhotelov, and O. Santolík (2007), Electron acceleration in the Van Allen radiation belts by fast magnetosonic waves, *Geophys. Res. Lett.*, *34*, L17107, doi:10.1029/2007GL030267.

Kim, H.-J., and A. A. Chan (1997), Fully adiabatic changes in storm time relativistic electron fluxes, *J. Geophys. Res.*, *102*, 22,107–22,116.

Loewe, C. A., and G. W. Prölss (1997), Classification and mean behavior of magnetic storms, *J. Geophys. Res.*, *102*, 14,209–14,213.

Meredith, N. P., R. M. Thorne, R. B. Horne, D. Summers, B. J. Fraser, and R. R. Anderson (2003), Statistical analysis of relativistic electron energies for cyclotron resonance with EMIC waves observed on CRRES, *J. Geophys. Res.*, *108*(A6), 1250, doi:10.1029/2002JA009700.

Millan, R. M., and R. M. Thorne (2007), Review of radiation belt relativistic electron losses, *J. Atmos. Sol. Terr. Phys.*, *69*, 362–377.

Onsager, T. G., G. Rostoker, H.-J. Kim, G. D. Reeves, T. Obara, H. J. Singer, and C. Smithtro (2002), Radiation belt electron flux dropouts: Local time, radial, and particle-energy dependence, *J. Geophys. Res.*, *107*(A11), 1382, doi:10.1029/2001JA000187.

Reeves, G. D., K. L. McAdams, R. H. W. Friedel, and T. P. O'Brien (2003), Acceleration and loss of relativistic electrons during geomagnetic storms, *Geophys. Res. Lett.*, *30*(10), 1529, doi:10.1029/2002GL016513.

Rozanov, E., L. Callis, M. Schlesinger, F. Yang, N. Andronova, and V. Zubov (2005), Atmospheric response to NO_y source due to energetic electron precipitation, *Geophys. Res. Lett.*, *32*, L14811, doi:10.1029/2005GL023041.

Sandanger, M. I., F. Soraas, M. Sorbo, K. Aarsnes, K. Oksavik, and D. S. Evans (2009), Relativistic electron losses related to EMIC waves during CIR and CME storms, *J. Atmos. Sol. Terr. Phys.*, *71*, 1126–1144.

Selesnick, R. S. (2006), Source and loss rates of radiation belt relativistic electrons during magnetic storms, *J. Geophys. Res.*, *111*, A04210, doi:10.1029/2005JA011473.

Shprits, Y. Y., R. M. Thorne, R. Friedel, G. D. Reeves, J. Fennell, D. N. Baker, and S. G. Kanekal (2006), Outward radial diffusion driven by losses at magnetopause, *J. Geophys. Res.*, *111*, A11214, doi:10.1029/2006JA011657.

Shprits, Y. Y., L. Chen, and R. M. Thorne (2009), Simulations of pitch angle scattering of relativistic electrons with MLT-dependent diffusion coefficients, *J. Geophys. Res.*, *114*, A03219, doi:10.1029/2008JA013695.

Summers, D., and R. M. Thorne (2003), Relativistic electron pitch-angle scattering by electromagnetic ion cyclotron waves during geomagnetic storms, *J. Geophys. Res.*, *108*(A4), 1143, doi:10.1029/2002JA009489.

Thorne, R. M. (1977), Energetic radiation belt electron precipitation: A natural depletion mechanism for stratospheric ozone, *Science*, *195*, 287–289.

Tsurutani, B. T., R. L. McPherron, W. D. Gonzalez, G. Lu, N. Gopalswamy, and F. L. Guarnieri (2006), Magnetic storms caused by corotating solar wind streams, in *Recurrent Magnetic Storms: Corotating Solar Wind Streams*, *Geophys. Monogr. Ser.*, vol. 167, edited by B. T. Tsurutani et al., pp. 1–17, AGU, Washington, D. C.

Varotsou, A., D. Boscher, S. Bourdarie, R. B. Horne, S. A. Glauert, and N. P. Meredith (2005), Simulation of the outer radiation belt electrons near geosynchronous orbit including both radial diffusion and resonant interaction with whistler-mode chorus waves, *Geophys. Res. Lett.*, *32*, L19106, doi:10.1029/2005GL023282.

R. B. Horne and M. M. Lam, British Antarctic Survey, Madingley Road, Cambridge CB3 0ET, UK. (rh@bas.ac.uk; mlam@bas.ac.uk)

J. C. Green, Space Weather Prediction Center, National Oceanic and Atmospheric Administration, 325 Broadway, Boulder, CO 80305-0000, USA. (janet.green@noaa.gov)